Semi-empirical framework for predicting the noise from wind-turbine blades with serrated trailing edges

AIAA AVIATION Forum
12-16 June 2023, San Diego, CA and Online
AIAA AVIATION 2023 Forum

10.2514/6.2023-3644

Semi-empirical framework for predicting the noise from wind-turbine blades with serrated trailing edges

Lourenço T. Lima Pereira*, Francesco Avallone†, and Daniele Ragni‡
*,†,‡*Delft University of Technology, Delft, The Netherlands, 2628 CD*
†*Politecnico di Torino, Torino, Italy, 10129*

Steven Buck§
Siemens Gamesa Renewable Energy, Boulder, Colorado 80303, United States

Stefan Oerlemans¶
Siemens Gamesa Renewable Energy, DK-7330 Brande, Denmark

This work proposes a semi-empirical framework to predict the noise of wind turbines with serrated trailing edge blades. The framework is employed for studying the reduction of the noise of the SWT 2.3-93 benchmark wind turbine. The framework is verified against field acoustic measurements of the real wind-turbine model and of noise reduction measured for airfoil geometries with serrated trailing edges. Two different serration design strategies are proposed, respectively one with the same serration geometry along the blade and one with serrations scaled with the local boundary-layer properties along the radius. Results show the predicted noise reduction obtained with each of the add-ons and explore the benefits of tailoring the design of the serrations according to the varying flow conditions along the blade span.

I. Nomenclature

x_1, x_2, x_3	=	Streamwise , wall-normal, and spanwise directions along the blade section
$2h$	=	Serration height
A_{ref}	=	Reference surface area (1 m^2)
c	=	Airfoil chord
f	=	Frequency
f_{A}	=	A-weighting coefficient
$f_{\text{abs.}}$	=	Atmospheric absorption coefficient
$f_{\text{cut-off}}$	=	Cut-off frequency of noise reduction
f_{load}	=	Frequency of maximum aerodynamic loading effect
$f_{\text{serr.}}$	=	Serration noise reduction coefficient
l_{x_3}	=	Spanwise correlation length
n_b	=	Number of blades in the wind turbine
s	=	Blade span
S_{ref}	=	Reference sound pressure level (4×10^{-10} Pa^2)
S_{pp}	=	Sound pressure level spectrum per metre from a blade-section
$S_{pp,\text{WT}}$	=	Sound pressure level spectrum of the wind turbine
U_c	=	Convective velocity of the wall-pressure fluctuations
U_{wind}	=	Wind speed
α	=	Airfoil angle of attack
λ	=	Serration wavelength

*Ph.D. candidate, Delft University of Technology, l.t.limapereira@tudelft.nl.
†Assistant professor, Delft University of Technology, Politecnico di Torino.
‡Associate professor, Delft University of Technology.
§Aeroacoustics Engineer, Siemens Gamesa Renewable Energy, 1050 Walnut St. Ste. 303.
¶Senior Key Expert Aeroacoustics, Siemens Gamesa Renewable Energy, Borupvej 16.

ν = Kinematic viscosity of the air
ψ = Blade elevation angle
ω = Radial frequency ($2\pi f$)

II. Introduction

A significant contribution to the noise of wind turbines comes from the interaction between the turbulent fluctuations from the boundary layer and the blade's trailing edge [1], known as turbulent boundary layer trailing-edge noise [2]. The use of trailing-edge serrations is a well known solution to mitigate this noise source [3]. By creating a non-orthogonal angle between the incoming turbulent fluctuations and the trailing edge, serrations can reduce the overall scattered noise of a wind turbine by more than 3 dB [3]. The reduced noise, combined with the negligible effects on the turbine performance, and the practicality of its application, make the solution the current standard for wind turbines.

Several studies have addressed the noise reduction from trailing-edge serrations [4–8], creating models that predict how the geometry impacts the acoustic scattering. However, these predictions differ from experimental evidence [8–10], indicating that the modelling of the relevant physics of noise reduction by trailing-edge serrations is not accurate. Research attributes these discrepancies to the flow conditions in the surroundings of the serration [11–15], that deviates from the supposed condition of pure advection at the trailing edge (Taylor's frozen turbulence [16]). References [13, 17, 18] indicated that accounting for the variation of the flow close to the serrations yields improvements in the noise reduction predictions from serrations. The work of Kholodov et al. [19] also showed that the theoretical optimal serration geometry varies with the scales of the turbulent boundary layer at the trailing edge. This was also demonstrated experimentally in previous parametric studies [10]. Opposite to what was predicted, the latter work observed that the serration dimensions for maximum noise reduction are more dependent on the turbulent boundary-layer scales than on the serration aspect ratio, i.e. the ratio between serration height ($2h$), and wavelength (λ).

The inconsistencies observed for the analytical predictions hamper their use for preliminary designing purposes. Thus, applications have to rely on high-fidelity numerical simulations [20, 21], and dedicated experimental campaigns of 2D wing sections [22], where fewer configurations can be assessed. For the particular case of wind-turbine applications, the varying flow conditions along the blade span also indicate that the optimal design is different for each span position. This translates to finding a serration geometry for each section of the blade that minimizes the far-field scattered noise.

This work explores a possible framework for the assessment and design of serrated trailing edges for wind-turbine applications. This framework is explored for the design assessment of trailing-edge serrations for the reduction of wind-turbine noise. The SWT 2.3-93 benchmark wind-turbine model is used as the reference geometry [23], to which blades, the serrations are designed. Validation of the methodology is provided by two means. First, the acoustic emissions of the baseline wind-turbine model without serrations are estimated analytically and compared against available acoustic measurements. Second, the noise reduction estimation for the serrations is validated against a wind-tunnel study carried out with different serration geometries. From the baseline acoustic noise, two serration design strategies are explored. A first design is based on a single serration geometry over the entire blade optimized for minimum noise while a second design is based on the scaling of the serrations with the boundary-layer thickness. The results discuss the expected noise reduction, benefits, and shortcomings of designing serrations based on the varying flow conditions along the wind-turbine blade. Section III describes the framework developed and main assumptions. Section IV describes the case studies, serration geometries tested, and the validation results. Results section (Section V) is dedicated to the comparisons between the two serration designs and the importance of designing serrations considering the spanwise flow variations along the blade.

III. Methodology

The framework developed in this work is divided into two parts, the first refers to the estimation of the reference wind-turbine noise without serrations. The second describes the modelling of the noise emissions from a blade with serrated trailing edges, emphasizing the specifics of modelling the noise reduction from the serrated trailing edge.

A. Trailing-edge noise from wind-turbine blades

The modelling of the noise emitted from the wind-turbine blade is based on the framework illustrated in Fig. 1. The estimation starts from partitioning the blade in sections along the span where the conditions are considered equal. For each of the sections, the acoustic spectrum from the turbulent boundary layer trailing-edge noise ($S_{pp}\left(\boldsymbol{x_o}, \omega\right)$)

is estimated following Amiet's [2] work (eq. 1) with back-scattering corrections from Roger & Moreau [24]. In the equation, x_o is the observer's location with respect to the spanwise section, $\mathcal{L}\left(\omega, k_1 = \omega/U_c, k_3 = 0, \boldsymbol{x_o}\right)$ is the acoustic transfer function, Δb, the spanwise extension of the section, ϕ_{pp} the wall-pressure spectrum of the turbulent fluctuations at the trailing edge, and l_{x3}, its spanwise correlation length.

This estimation requires a model for the wall-pressure spectrum and spanwise correlation length from the turbulent fluctuations of the boundary layer. For the wall-pressure spectrum, 4 models are used in this work, namely the Goody [25], Kamruzzaman [26], Lee [27], and Rozenberg [28]. These 4 models are selected based on the available dataset and suitability for different flow conditions. The model of Corcos [29] is selected for the spanwise correlation length, where the semi-empirical coefficients are taken from the work of Hu & Herr [30]. These semi-empirical models are based on the properties of the boundary layer at the trailing edge of the blade section, taken as input to the framework.

$$S_{pp}\left(\boldsymbol{x_o}, \omega\right) = \left|\mathcal{L}\left(\omega, k_1 = \omega/U_c, k_3 = 0, \boldsymbol{x_o}\right)\right|^2 \phi_{pp}\left(\omega\right) l_{x3}\left(\omega\right) \Delta b. \tag{1}$$

The predicted noise emissions from a blade section are corrected with the estimation of the atmospheric absorption, following ISO 9613-1. The noise of the blade is determined by the numerical integration along the span. The noise of the wind-turbine blade must also consider the different azimuthal positions (ψ) as the blade rotates. This translates to an average over the blade rotation. The A-weighted wind-turbine noise ($S_{pp,\mathrm{WT}}\left(\omega, \boldsymbol{x_o}\right)$) at a given location $\boldsymbol{x_o}$ is then estimated according to eq. 2, where n_b is the number of blades, f_A the non-dimensional A-weighting coefficient, $f_{\text{abs.}}$ the absorption coefficient, and $f_{\text{serr.}}$ the attenuation coefficient from the serrated trailing edge.

$$S_{pp,\mathrm{WT}}\left(\omega, \boldsymbol{x_o}\right) = n_\mathrm{b} \frac{1}{2\pi} f_A\left(\omega\right) \int_0^{2\pi} \int_0^b S_{pp}\left(\omega, \boldsymbol{x_o}, x_3, \psi, 2h, \lambda\right) f_{\text{serr.}}\left(\omega, 2h, \lambda\right) f_{\text{abs.}}\left(\omega, \boldsymbol{x_o}, x_3, \psi\right) dx_3 d\psi. \tag{2}$$

A final consideration for the comparisons is the conversion to sound power level (SWL) from the sound pressure levels (SPL). This is achieved by considering the wind turbine as a spherical source at the hub location, following eq. 3, where R_o is the distance between the turbine hub and the observer. This procedure is the same as the adopted one for the acoustic measurements from the baseline wind-turbine model [31]. The overall sound power level ($OASWL$) is estimated from the integral of the sound power spectrum, following eq. 4.

$$SWL = 10\log_{10}\left(\frac{S_{pp,\mathrm{WT}}}{S_\mathrm{ref}}\right) + 10\log_{10}\left(\frac{4\pi {R_o}^2}{A_\mathrm{ref}}\right). \tag{3}$$

$$OASWL = 10\log_{10}\left(\frac{\int S_{pp,\mathrm{WT}}\left(\omega\right) d\omega}{S_\mathrm{ref}}\right) + 10\log_{10}\left(\frac{4\pi {R_o}^2}{A_\mathrm{ref}}\right). \tag{4}$$

1. Noise reduction from serrated trailing-edge blades

The noise reduction achieved by the serration add-ons is estimated as a superposition of two independent effects. The first is the modification the add-on imposes on the scattering transfer function ($\mathcal{L}\left(\omega, k_1 = \omega/U_c, k_3, \boldsymbol{x_o}\right)$). This can be modelled following the works of Howe [4] and Lyu & Ayton [6–8].

To this model, the alterations of the flow imposed by the serration must be considered. Especifically, the modification of the wall-pressure spectrum in the vicinity of the serration surface [13, 32–35] must be accounted for. This follows the work of Lima Pereira et al. [36] which proposed the physical mechanisms and semi-empirical models to describe the alterations on the wall-pressure fluctuations along the edges of the serrations. Fig. 1 shows the modified framework used for the prediction of the wind-turbine noise with serrated trailing-edge add-ons. The red text highlights the main modifications to the straight trailing edge prediction model.

Two modifications of the wall-pressure fluctuations are considered in this framework, e.g. the wake development along the blade and the effect of the incidence angle of the blade, which causes vortex pairs to form along the serration gaps. The first effect refers to the flow acceleration and development along the space between the serrations. This causes the convective velocity to increase between the root and tip of the serrations, in turn causing an increase in the incoming wall-pressure fluctuations. The modification of the convective velocity is considered following eq. 5, [36]. From the modified convective velocity, the wall-pressure fluctuations at the serration are estimated and used for the acoustic predictions, following eq. 6, [36]. The development of the wake causes a cut-off in the noise reduction spectrum and is more prominent at frequencies above $f_{\text{cut-off}} = 0.05\frac{{u_\tau}^2}{\nu}$, determined by the inner scales of the boundary layer.

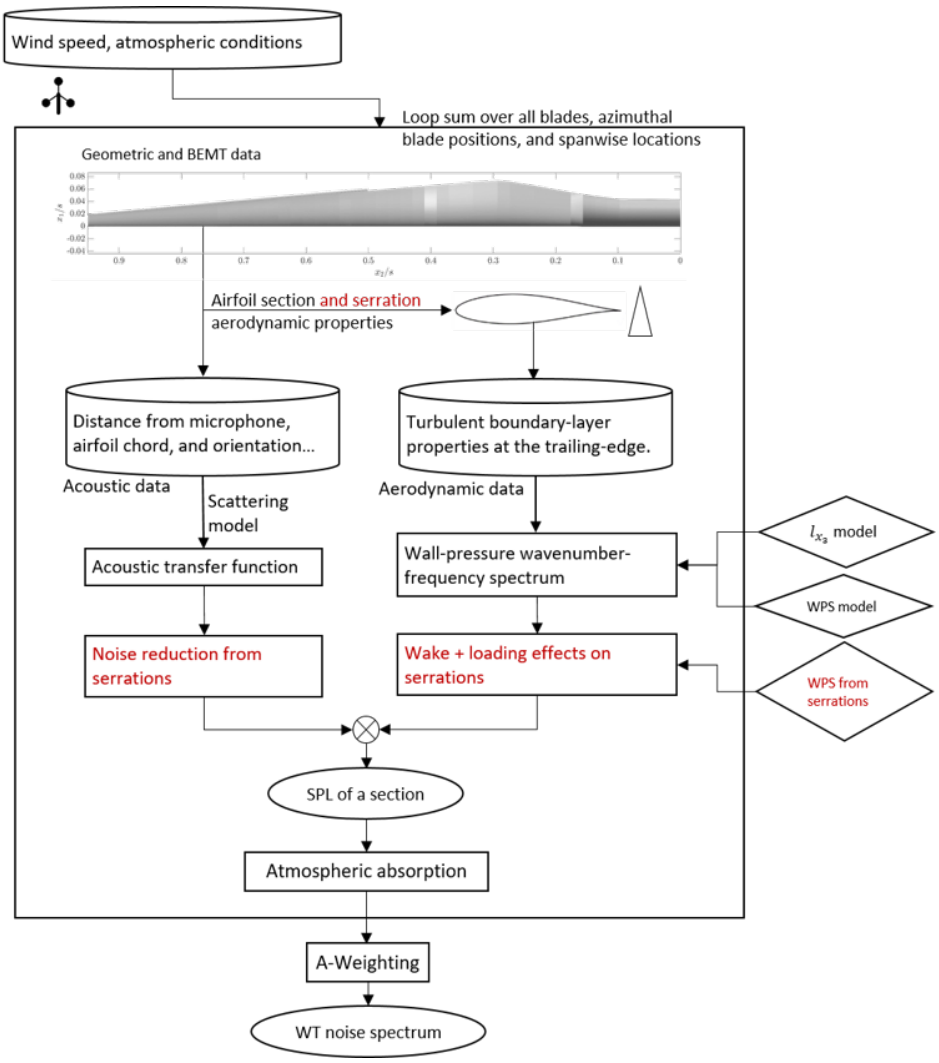

Fig. 1 Flowchart of the procedure for estimating the acoustic levels of the wind-turbine model. Modifications due to the application of serrated add-ons on the blades are highlighted in red.

$$\frac{U_{c,\text{wake}}}{U_e} = 1 + 1.55\,(2h)\,. \tag{5}$$

$$\frac{\phi_{pp,\text{wake}}}{\phi_{pp,\text{TBL}}}(\omega) = \frac{1 + 1.1^7 R_t{}^{-4}\left(\frac{\omega\delta}{U_{c,\text{TBL}}}\right)^5}{1 + 1.1^7 R_t{}^{-4}\left(\frac{\omega\delta}{U_{c,\text{wake}}}\right)^5}. \tag{6}$$

The second effect considered is the one of aerodynamic loading due to the angle between the flow and the serration. The wall-pressure fluctuations induced by the aerodynamic loading are superposed to the one of the turbulent boundary layer corrected by the wake effect, as in eq. 7 [36], where $St_{\delta^*} = \frac{f\delta^*}{U_e}$, *erfc* is the complementary error function, and α_s is the serration angle of attack (eq. 8, [36]). In the equation, α is the section angle of attack, δ_{TE} is the airfoil trailing-edge angle, δ_{camber} the camber angle, δ_{flap} the serration flap angle, and θ the blade section twist. It is important to point out that the wall-pressure fluctuations increase proposed in eq. 7 has a maximum at a frequency given by eq. 9, [36].

$$\phi_{pp,\text{Load}} = 5.1 \times 10^{-3} \left(\rho {U_e}^3 \delta^*\right) {\alpha_s}^2 \left[\left(\frac{2h}{\lambda}\right)^2 + \frac{1}{4}\right] \left(St_{\delta^*} - \frac{1}{4}\frac{\delta^*}{2h}\right)^2 \text{erfc}\left[2.5\left(St_{\delta^*} - \frac{1}{4}\frac{\delta^*}{2h}\right)\right]. \tag{7}$$

$$\alpha_s = \alpha + \delta_{\text{TE}} + \delta_{\text{camber}} + \delta_{\text{flap}} + \theta. \tag{8}$$

$$\frac{f_{\text{load}}\delta^*}{U_\infty} = \frac{1}{4}\frac{\delta^*}{2h} + \frac{\sqrt{\pi}}{5}. \tag{9}$$

B. Assumptions

Considerations are made for the current noise prediction method of the wind-turbine noise. These hypotheses can impact the estimated baseline levels of the wind turbine, but also the serration designs obtained. The following four considerations and possible impacts on the results obtained are made in this model:

- **Trailing-edge noise is the only source of noise:** The current technique is devoted to studying the reduction of trailing-edge noise using serrated trailing-edge inserts. For that, the current methodology only considers this source of noise from a wind turbine. Other sources of noise, such as inflow-turbulence interaction noise [37], can affect the final noise spectrum and consequently, the minimization results shown in this work;
- **Doppler effect is disregarded:** The Doppler effect caused by the relative blade movement with respect to the observer is disregarded in this work. The reasons are the far downstream distance of the reference position and the low blade speed of the test case used (Section IV). The Doppler effect causes a shift of the frequency spectrum, which can impact the optimal geometry of the serration;
- **Flow convection is disregarded:** The convection of acoustic waves due to the wind speed is disregarded in this work given the low wind speeds considered (below 15 m/s). This consideration can alter the levels predicted of the wind-turbine noise.
- **Noise from other non-zero spanwise wavenumbers is neglected:** For the baseline configurations, the scattering from non-zero spanwise wavenumbers is neglected. This assumption is equivalent to the consideration of Amiet [2] for large spans in comparison to the spanwise correlation length. This assumption might change the estimation of the baseline levels, with no effect on the noise reduction predicted.

IV. Case studies and validation of the framework

A. Wind-turbine model

The SWT 2.3-93 wind turbine model is selected for this study. The turbine has a 93 m diameter and a rated power of 2.3 MW. Geometric and acoustic information on the turbine is made available in the benchmark dataset from the zEPHYR H2020 project [23]. The benchmark data includes an equivalent rotor design [38], and field acoustic measurements for the baseline wind turbine [31]. Fig. 2a illustrates the wind turbine model, while Fig. 2b shows the velocity vs. blade rotational speed assumed for the model.

The acoustic measurements from the real turbine were conducted with a microphone probe located 100 m downwind from the wind-turbine tower. The data used refers to two wind speed conditions, namely $U_{\text{wind}} = 6$, and 9.5 m/s. Under these conditions, the reported rotational speeds are respectively 13, and 17 RPM. The latter flow speed is taken as reference for this work as it gives maximum sound power emissions.

B. Serration set designs

Two serration design approaches are explored in this study. The designs are based on the noise emissions under the wind speed of 9.5 m/s, representative of a maximum RPM condition where baseline acoustic results exist. The first serration set is based on a single sawtooth serration geometry in the entire blade span. The geometry is determined following a minimization of the Overall Sound Power Levels at 9.5 m/s wind speed. Following the work of Lima Pereira et al. [39], an aspect ratio of the serration ($2h/\lambda$) around 2 (eq. 10) is selected. In this way, the minimization is based on a single parameter, i.e. the serration height, according to eq. 11.

$$\lambda = \frac{1}{2}2h. \tag{10}$$

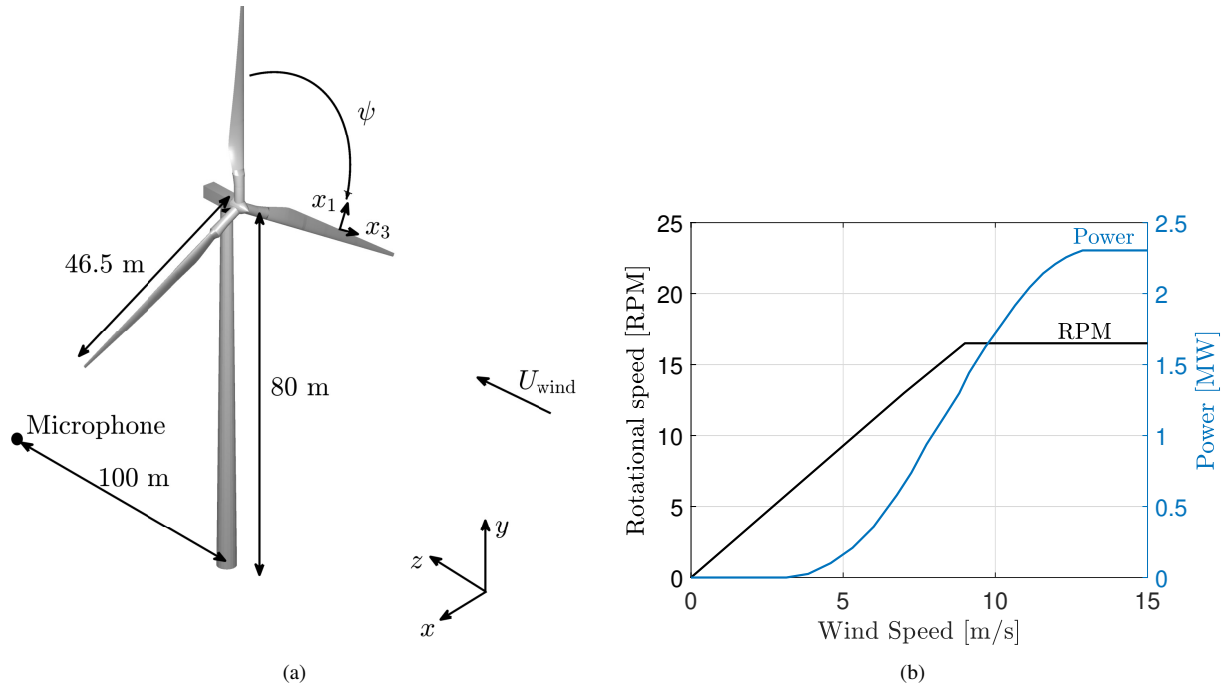

Fig. 2 Wind-turbine model and operational curves [38].(a) illustrates the wind-turbine geometry, dimensions, and axes. (b) shows the turbine RPM and power curve per wind speed.

$$\min_{2h} OASWL \tag{11}$$

The second set of serrations follows a typical scaling with the boundary-layer parameters. According to the works of Gruber et al. [10] and Lima Pereira et al. [39], a serration geometry for maximum noise reduction should be higher than 12 times boundary-layer displacement thickness (δ^*) and wider than 6 times the same thickness. A minimum serration within those conditions can be designed according to eqs. 10 and 12. Therefore, the design only requires information on the boundary-layer displacement thickness along the blade span, and no minimization procedure is required.

$$2h = 12\delta^*. \tag{12}$$

Fig. 3 shows the resulting serration height from the two serration designs normalized by a reference height, taken as the one of the single serration geometry. The scaling with the boundary layer produces serrations that are significantly bigger (more than twice the height) at the inboard section of the blade in comparison to the single serration design. Both designs are equal at around 95% of the blade span.

C. Baseline wind-turbine noise levels

From the framework described, the baseline noise of the wind-turbine model is estimated. Fig. 4 shows the acoustic spectra predicted against the measurements provided by the benchmark at 6 (13 RPM), and 9.5 m/s (17 RPM). For the predictions, 4 different wall-pressure spectrum models are used, namely Goody [25], Kamruzzaman [26], Lee [27], and Rozenberg [28]. The results show that the methodology proposed is able to accurately describe the measured spectrum from the wind turbine for both wind speeds where data is available. Among the wall-pressure spectrum models, the one of Kamruzzaman is the one that better agrees with the measurements, and is therefore selected for the remainder of the analyses. At low frequencies, the models underestimates the acoustic levels. According to [37], this can be caused by the interaction between the blade and the atmospheric turbulence, which is another source of wind-turbine noise that can be dominating in the low frequencies.

The contour plots in Fig. 5 show the contribution to the noise of each radial section of the blade versus frequency. Figs. 5a, and b, show the sound power level in frequency for each blade section along the span, with respect to the

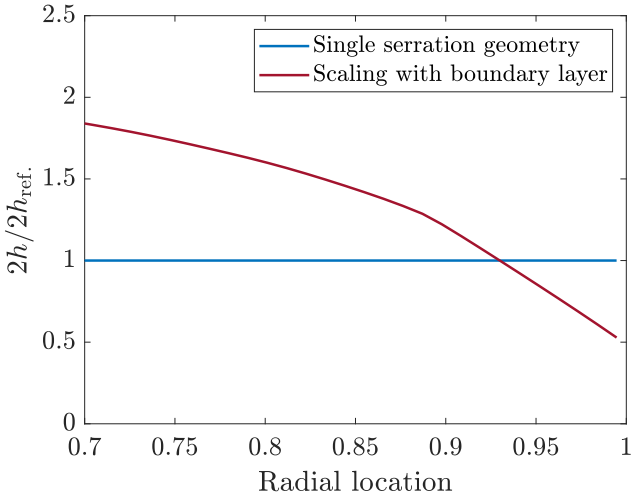

Fig. 3 Serration height for both designs normalized by the height of the single serration geometry.

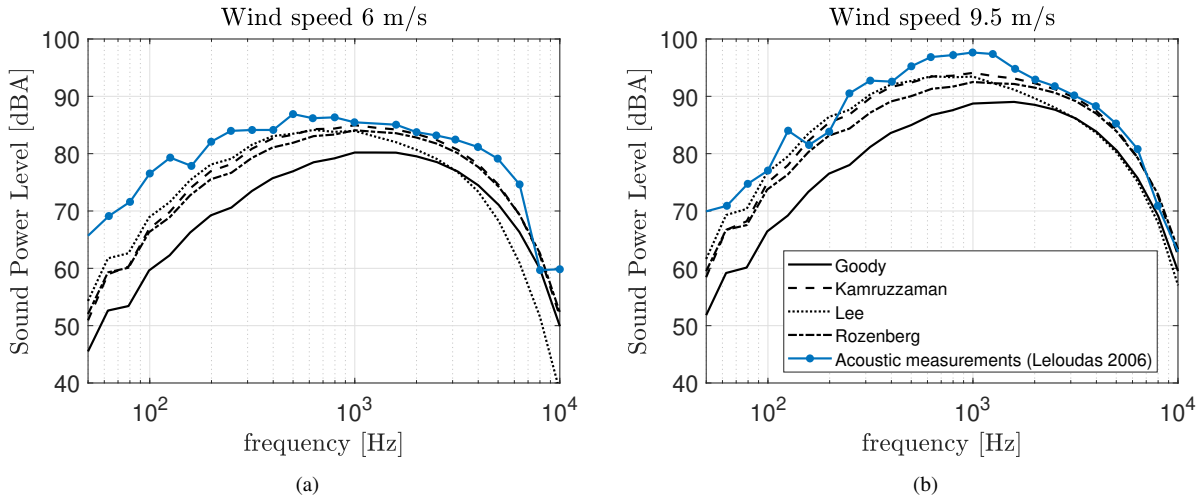

Fig. 4 Predicted wind-turbine Sound Power Level for an observer 100 m downwind from the wind turbine using different wall-pressure spectrum models for two different wind speeds, 6 m/s (a), and 9.5 m/s (b) respectively. Acoustic measurements from [31] are also shown in blue lines.

maximum level among all the frequencies. The noise produced, for both speeds, has a maximum at around 500 Hz. Nevertheless, significant noise contributions are also found from 200 Hz to 1500 Hz (between 3 dB from the maximum), indicating a broad contribution of frequencies to the noise of the wind turbine. This region of maximum noise is found, for both cases, around 95% of the blade span, where the local flow speed is close to maximum.

Fig. 6 shows the predicted overall sound power level (OASWL) for different wind speeds. As shown in the figure, the noise from the turbine increases with wind speed approximately up to the speed of maximum rated RPM after which, for higher wind speeds, the noise levels remain constant.

The same figure also reveals how the frequency where the noise spectrum is maximum varies with speed. It is important to point out that the frequency of maximum noise does not match the one of Fig. 4 due to the one-third-octave band representation used in the latter. The frequency of maximum noise displays different behaviour with speed. At speeds lower than 5 m/s, the frequency is reduced with the wind speed. For speeds above 5 m/s, the frequency of maximum noise increases up to approximately the region of constant RPM, above which, it reduces again until it reaches 12 m/s. Above this speed, the frequency of maximum noise is increased again. Overall, the frequency of maximum noise

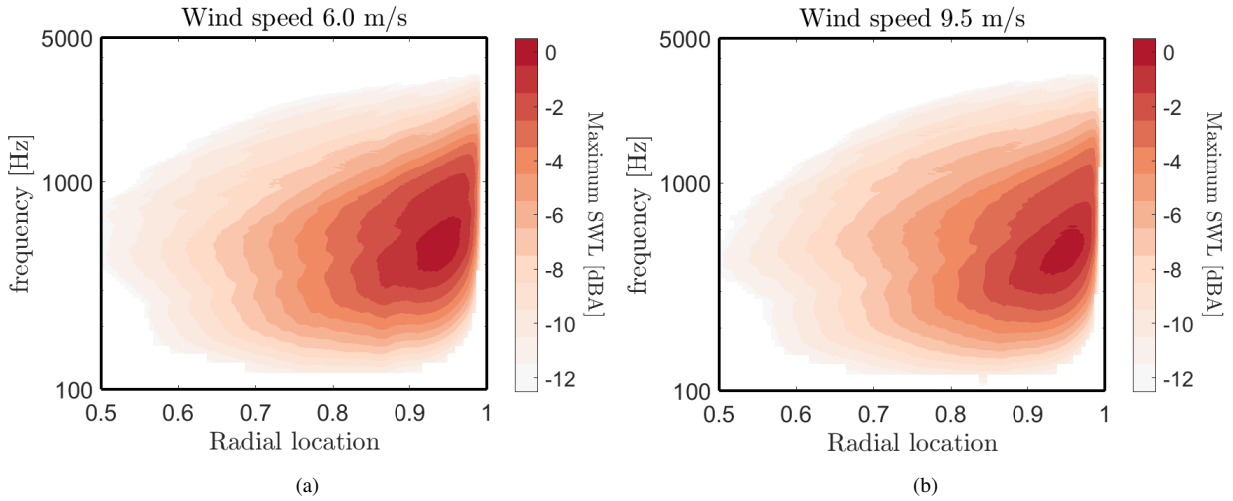

Fig. 5 Sound power level narrowband spectrum contribution along the normalized radius of the blade for an observer 100 m downstream from the wind turbine. (a), and (b) show the levels normalized by the maximum level obtained at all frequencies, and all radii for the wind speeds of 6 m/s, and 9.5 m/s respectively.

is above 300 Hz and below 1000 Hz, reaching frequencies higher than 600 Hz only along the constant RPM regime.

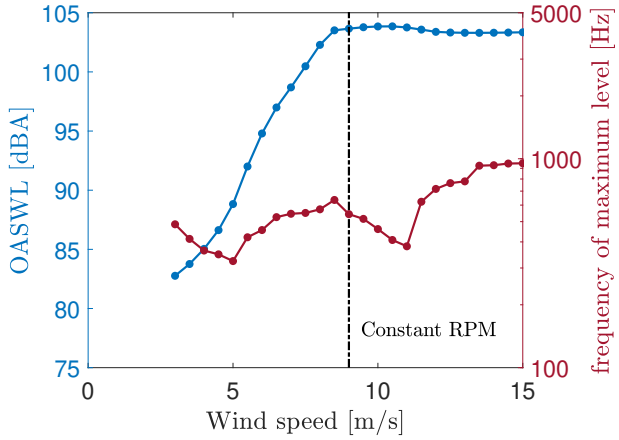

Fig. 6 Predicted variation of Overall Sound Power Level (OASWL), and frequency of maximum sound power level with the wind speed.

The contribution of each part of the blade to the overall sound power of the turbine is shown in Fig. 7 for wind speeds of 6, 9.5, and 13 m/s. The figure shows that the noise produced is maximum around 90-97% of the blade span. Moving outboard from that region, the boundary-layer thickness, and consequently the noise, reduces significantly. Moving inboard from the maximum noise generation region, the lower flow speeds cause significantly lower noise levels. As the wind speed increases, and the turbine enters the fixed RPM regime, the region of maximum noise is moved inboard, following the influence of the wind speed and the thickening of the boundary layer in the inboard region.

D. Noise reduction from different serration geometries

Validation of the methodology for the estimation of the noise reduction obtained with different serration geometries follows the results of the parametric wind-tunnel study shown in Lima Pereira et al. [39]. The study provides the acoustic noise reduction spectrum of several serration geometries attached to a benchmark NACA 63_3-018 airfoil section model.

Fig. 9 shows the predicted and measured noise reduction spectrum for changes made to the sawtooth serration height

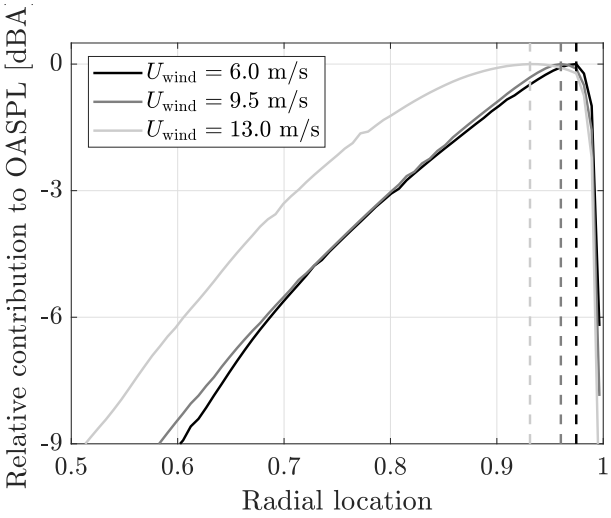

Fig. 7 Relative overall wind-turbine sound power level contribution per section of the blade span at different wind speeds.

($2h$), wavelength (λ), and scale (fixed $2h/\lambda$, different $2h$ and λ) for a low aerodynamic loading condition ($\alpha = 0^o$). The ΔSPL is defined as the difference between the serrated airfoil and the baseline one. Therefore, a negative value in the spectrum indicates noise reduction while a positive one means an increase in noise levels.

The model proposed can describe the changes observed for each of the modifications applied to the sawtooth serration design. In Fig. 9a, the increase in serration height yields an increase in the noise reduction obtained. Predictions for this case are better for the high values of serration height ($2h$ = 30 and 40 mm) and underpredict noise reduction for the low values of serration height ($2h$ = 10, and 20 mm). In Fig. 9b the modification of the serration size (with the same aspect ratio) is well captured by the predictions. Underprediction of the noise reduction is only observed for the smallest of the serrations tested, $2h$ = 10 and λ = 5 mm. In Fig. 9c, the change in serration wavelength is observed. As measured and predicted, decreasing the wavelength does not translate to an increase in noise reduction [39]. This is due to the change in the frequency range where noise reduction is captured. The smaller the serration wavelength is, the higher the cut-on frequency, the frequency at which noise reduction starts to ramp up. However, the cut-off due to the aerodynamic wake development remains the same, therefore the lower the total noise reduction achieved. Again, the noise reduction is underpredicted for the smallest of the wavenumbers tested (λ = 5 mm). The underpredicted cases represent conditions far outside from the envelope of serration design, where the serrations are small with respect to the boundary-layer thickness. Thus, the discrepancies are deemed acceptable for this study.

When placed at angles, serrations present a different behaviour as the aerodynamic loading of the serrations causes the noise reduction to decrease at high frequencies. Figure 9(a) shows the predictions obtained at high angles of attack with different serrations sizes while Figure 9(b) shows the predictions for a single geometry at $\alpha = 0°$, and $10°$. The predictions are also able to describe the impact of the serration angle on the noise reduction spectrum achieved, illustrating the accuracy of the current framework for predicting the noise reduction from different serration geometries and flow conditions.

V. Acoustics of the wind turbine with different serration designs

The results section focuses on the comparison between the serration strategies proposed and the differences between the noise emissions of each design. Fig. 10 shows in blue the spectrum of noise emissions from the baseline blade (solid line) and from the two serration sets (dashed and dotted lines respectively). The differences between the acoustic spectrum of the different serration designs and the baseline one evidences the noise reduction obtained. Despite the small differences between the two serrations, it is evident when comparing the designs that the variable serration design is more effective in reducing noise at lower frequencies. Fig. 10 also shows, in red lines on the right axis, the noise reduction spectrum promoted by the two designs. The graph reveals how the scaled serration design is able to reduce the noise around a broader range of frequency. In particular, this design reduces more noise at lower frequencies when

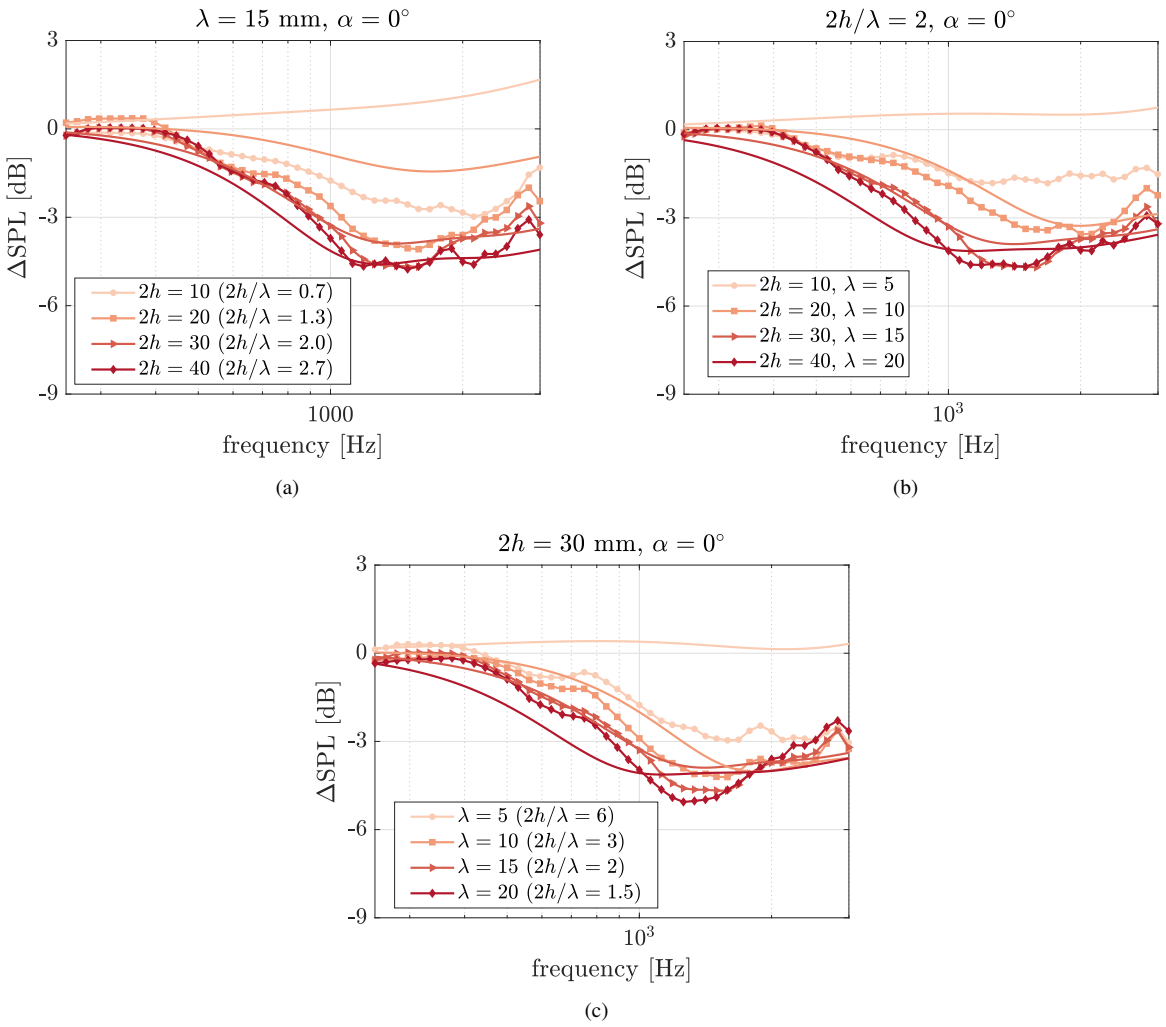

Fig. 8 Predicted (solid line) and measured (line with markers) noise reduction from serrated trailing edges mounted on a symmetric benchmark airfoil NACA 63_3-018 at zero angle of attack (dimensions in millimiters). (a) shows the predicted noise reduction variation with changing serration height (same serration wavelength, $\lambda = 15$ mm). (b) shows the predicted noise reduction variation with changing serration size (same serration aspect ratio, $2h/\lambda = 2$). (c) shows the predicted noise reduction variation with changing serration wavelength (same serration height, $2h = 30$ mm).

compared to the single serration design, with a frequency of maximum noise reduction closer to the frequency of maximum noise of the baseline noise (520 Hz), shown by the black dashed line in the graph. At higher frequencies, both designs perform similarly. This means that the scaled serration design is more tailored to reduce noise in the frequency range where the noise produced by the turbine is maximum.

The single serration design (dashed lines) is the one that reduces the noise the least. The boundary-layer scaled design (dotted lines) is the best-performing serration at lower frequencies. These results can be summarized in the overall noise reduction achieved with each of the serration sets in Tab. 1. The single serration design is able to reduce the overall sound power levels (OASWL) by 3.2 dB while the design based on the boundary-layer thickness reduces the noise levels by 3.5 dB, 0.3 dB more than the single serration.

This trend is seen to be kept when the same serration designs are tested at different wind speeds. Fig. 11 shows the variation of the overall sound power level and the reduction of the overall sound power level for the wind turbine with each of the serration designs. The noise reduction follows the same trend for the two serration designs. The only observed difference is the better performance of the serration based on the boundary-layer thickness for wind speeds

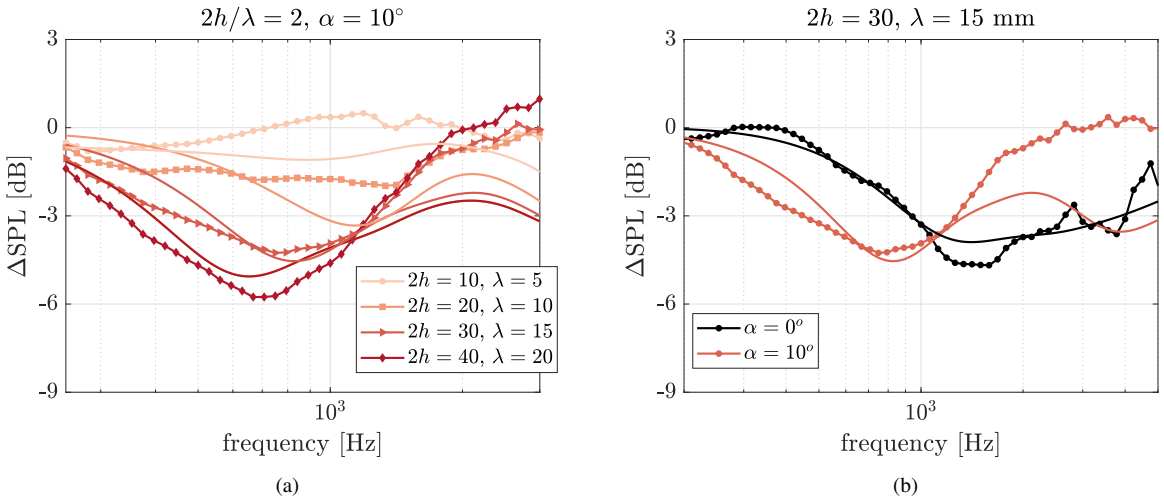

Fig. 9 Predicted and measured noise reduction from serrated trailing edges mounted on a symmetric benchmark airfoil NACA 63_3-018 at different angles of attack (dimensions in millimeters). (a) shows the predicted noise reduction variation with changing serration height (same serration wavelength, $\lambda = 15$ mm). (b) shows the predicted noise reduction variation with changing serration size (same serration aspect ratio, $2h/\lambda = 2$). (c) shows the predicted noise reduction variation with changing serration wavelength (same serration height, $2h = 30$ mm).

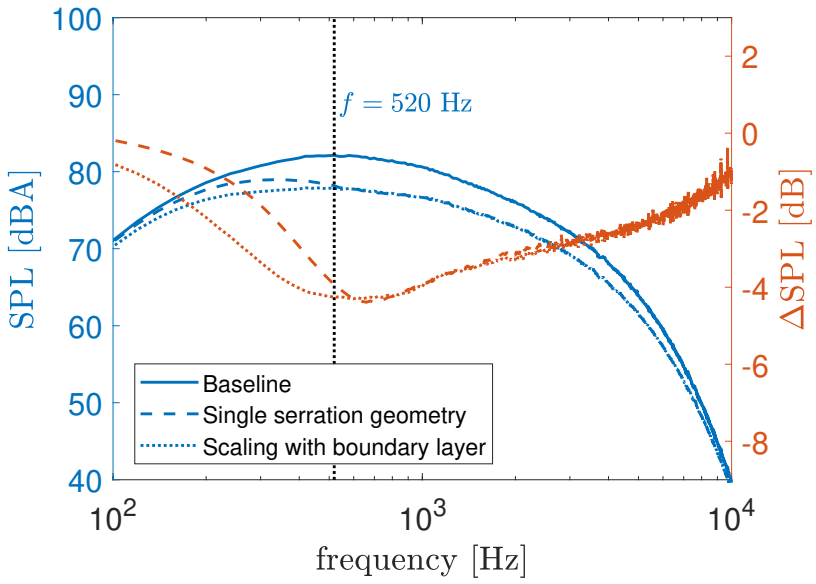

Fig. 10 Comparison of the noise reduction spectrum of the different serration designs presented in this work (a). (b) displays also the noise reduction spectrum. The dashed black line shows the frequency of maximum noise produced by the wind turbine.

above 12 m/s (fixed RPM regime). It is here speculated that the smaller serrations at the blade tip are more efficient in reducing noise at high local angles of attack of the blade sections.

A breakdown of noise generation and reduction per spanwise section is shown in Fig. 12. Fig. 12a-d shows the baseline emission spectrum and noise reduction at 70, 80, 90, and 95% of the blade span respectively. The left axis shows the noise spectrum from the straight trailing edge blade section, and the right axis shows the noise reduction spectrum obtained from each of the serration designs. The graph demonstrates how the different designs perform at

	Baseline	Single serration	Scaling with boundary layer
OASWL (dBA)	100.8	97.6	97.3
ΔOASWL (dBA)		-3.2	-3.5

Table 1 Overall noise levels and noise reduction achieved by the serration sets.

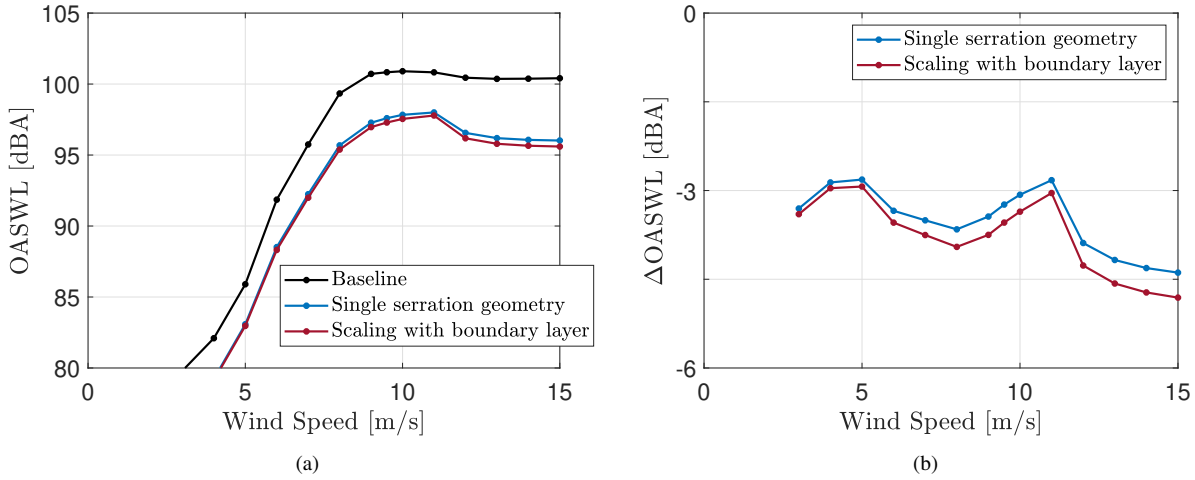

Fig. 11 Comparison of the overall sound power from the wind turbine under different wind speeds. (a) shows the overall sound power level (OASPL) and (b) the reduction of it (ΔOASPL) for the different serration designs.

different sections of the wind-turbine blade. It is interesting to observe how the two designs perform similarly in the outboard section of the blade, i.e. at 90 and 95% of the span (12c and d), following the similar serration sizes at this location. On the other hand, the larger serrations at the inboard sections, see 70 and 80% of the span (12a and b), of the scaled design are able to to reduce noise at lower frequencies, more in agreement with the noise emission spectrum from these sections of the blade. The results indicate that the optimization procedure used to size the single geometry prioritizes the noise reduction at the outboard sections of the blade, where more noise is generated. By scaling the serration design with the boundary-layer thickness along the blade, the noise reduction in the inboard sections are improved and the overall noise is reduced even further.

Fig. 13 shows the contours of noise reduction with radial position and frequency for each one of the designs proposed. Here, it is more evident the difference between the designs studied. The single serration design is effective in reducing noise at high frequencies. However, the noise levels below 500 Hz are not attenuated of the same intensity as the high frequency ones. Besides, the region of highest noise intensity in Fig. 13b is spread from 85 to 95% of the blade span. This indicates that the contribution of the inboard sections of the blade is as significant as the outboard ones with this serration design. Scaling the serration geometry with the boundary-layer thickness reduces significantly the noise produced in the inboard sections of the blade, resulting in a reduction of the trailing-edge noise over a broader range of frequencies and along the entire blade span, and consequently creating a design that generates lower noise.

VI. Conclusions

This work proposes a semi-analytical framework to design trailing-edge serrations for broadband noise reduction of wind turbines. This framework is tested for the benchmark geometry based on the SWT 2.3-93 wind-turbine model, where acoustic data is also available.

The baseline noise is estimated based on Amiet's method with back-scattering corrections. The wall-pressure wavenumber-frequency spectrum is obtained from semi-analytical methods, which require information on the turbulent boundary-layer properties around the trailing edge. The estimations yield good comparisons against the measurements at 6 m/s and 9.5 m/s wind speeds. The methodology is also used to assess the different sections along the blade where noise is produced and the frequencies where noise is maximum. The emissions from serrated trailing edge add-ons are

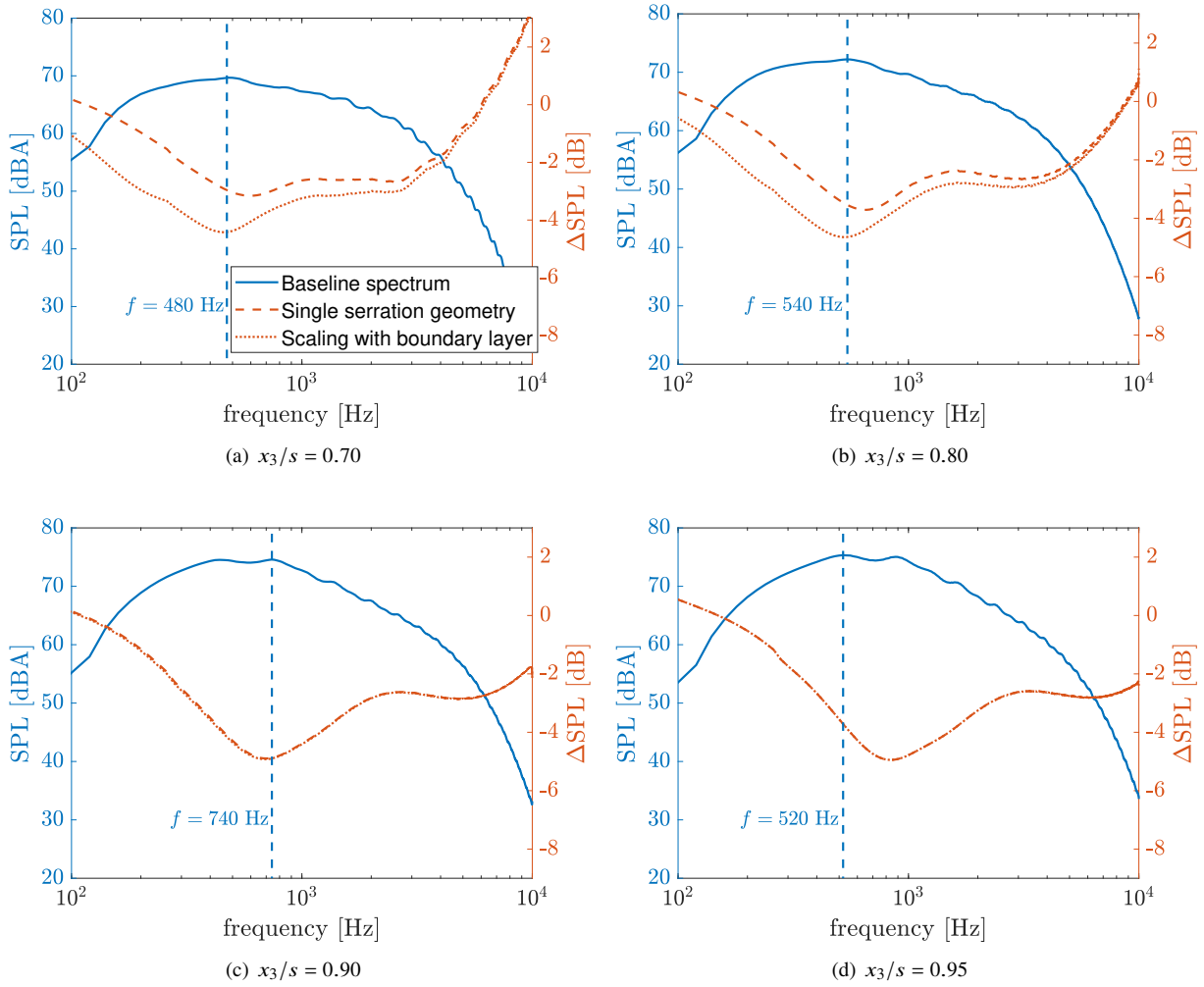

Fig. 12 Noise spectrum and noise reduction spectrum contribution from different spanwise sections of the wind-turbine blade with the two serrations sets designed. The blue dashed line indicates the frequency where TE noise is maximum.

predicted by considering both the effect of the add-ons on the scattering efficiency and on the wall-pressure fluctuations over the add-on surface. Estimations are compared against existing wind-tunnel studies to show the sensitivity of the method to different serration geometries.

Two different designs are proposed, one with a fixed serration geometry and size, and another where the serration is scaled with the boundary-layer thickness along the blade span. The results focus on the description of the noise reduction achieved from each of the serration designs. The single serration geometry is able to reduce the overall noise levels of the wind turbine by 3.2 dB. This design is effective in reducing noise at high frequencies. However, the noise reduction spectrum shows that the frequency of maximum noise reduction does not match the one where noise produced by the baseline is maximum, showing that modifications in the geometry along the blade can result in a more tailored design for the application.

The second design follows the thickness of the boundary layer along the blade span. This indicates that bigger serrations are installed at the inboard sections of the blade and smaller ones at the tip of the blade. This design is able to reduce the overall noise levels of the wind turbine by 3.5 dB. It is shown that this design is more suited for the reduction of the wind-turbine noise in the inboard sections, up to 80% of the blade span, and noise reduction at low frequencies is significantly improved with respect to a single serration geometry over the entire blade span. The results indicate the importance of considering the changing flow and acoustic conditions along the blade radius for the design of optimal

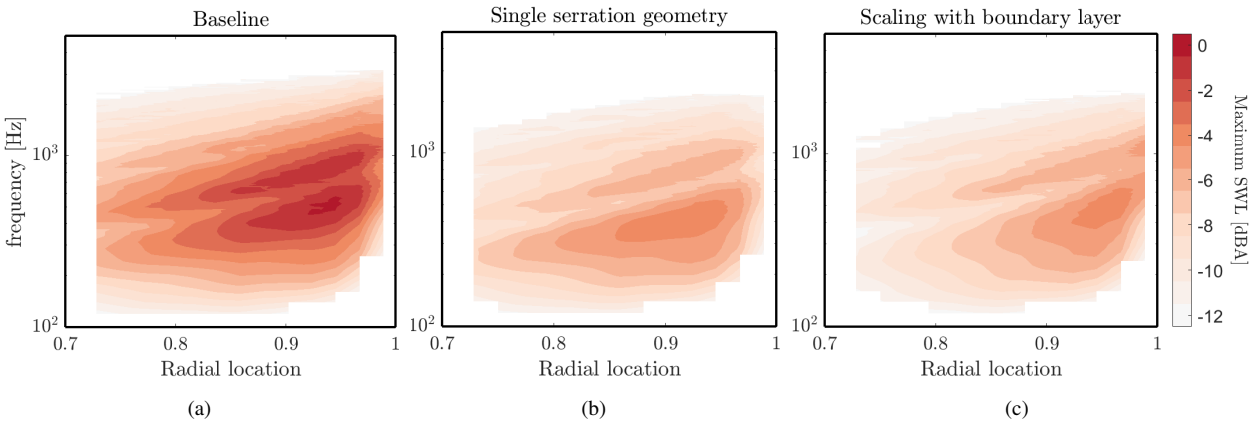

Fig. 13 Comparison of the noise emission contour spectrum over the blade span for the baseline (a), single serration geometry (b), and serrations scaling with the boundary layer (c). Reference is set to the maximum level of the baseline case.

serrated trailing-edge add-ons to minimize the wind-turbine noise. The framework developed in this work can be further explored for assessing the design of trailing-edge serrations for minimizing the noise produced by a wind-turbine blade.

Acknowledgments

This study is supported by the SMARTANSWER project which has received funding from the European Union's Horizon 2020 research and innovation program under the Marie Skłodowska-Curie grant agreement No. 722401. More information can be found at https://www.h2020-smartanswer.eu. The authors would like to acknowledge Oriol Ferret Gasch, and Pranav Manjunath for their assistance with the data gathering, and the fruitful discussions and guidance.

References

[1] Oerlemans, S., Sijtsma, P., and Méndez López, B., "Location and quantification of noise sources on a wind turbine," *Journal of Sound and Vibration*, Vol. 299, No. 4-5, 2007, pp. 869–883. https://doi.org/10.1016/j.jsv.2006.07.032.

[2] Amiet, R. K., "Noise due to turbulent flow past a trailing edge," *Journal of Sound and Vibration*, Vol. 47, No. 3, 1976, pp. 387–393. https://doi.org/10.1016/0022-460X(76)90948-2.

[3] Oerlemans, S., Fisher, M., Maeder, T., and Kögler, K., "Reduction of Wind Turbine Noise Using Optimized Airfoils and Trailing-Edge Serrations," *AIAA Journal*, Vol. 47, No. 6, 2009, pp. 1470–1481. https://doi.org/10.2514/1.38888, URL http://arc.aiaa.org/doi/10.2514/1.38888.

[4] Howe, M., "Aerodynamic noise of a serrated trailing edge," *Journal of Fluids and Structures*, Vol. 5, No. 1, 1991, pp. 33–45. https://doi.org/10.1016/0889-9746(91)80010-B, URL https://linkinghub.elsevier.com/retrieve/pii/088997469180010B.

[5] Howe, M. S., "Noise produced by a sawtooth trailing edge," *The Journal of the Acoustical Society of America*, Vol. 90, No. 1, 1991, pp. 482–487. https://doi.org/10.1121/1.401273.

[6] Lyu, B., Azarpeyvand, M., and Sinayoko, S., "Prediction of noise from serrated trailing edges," *Journal of Fluid Mechanics*, Vol. 793, 2016, pp. 556–588. https://doi.org/10.1017/jfm.2016.132.

[7] Ayton, L. J., "Analytic solution for aerodynamic noise generated by plates with spanwise-varying trailing edges," *Journal of Fluid Mechanics*, Vol. 849, No. August, 2018, pp. 448–466. https://doi.org/10.1017/jfm.2018.431.

[8] Lyu, B., and Ayton, L. J., "Rapid noise prediction models for serrated leading and trailing edges," *Journal of Sound and Vibration*, Vol. 469, 2020, p. 115136. https://doi.org/10.1016/j.jsv.2019.115136, URL https://doi.org/10.1016/j.jsv.2019.115136.

[9] Arce León, C., Ragni, D., Pröbsting, S., Scarano, F., and Madsen, J., "Flow topology and acoustic emissions of trailing edge serrations at incidence," *Experiments in Fluids*, Vol. 57, No. 5, 2016. https://doi.org/10.1007/s00348-016-2181-1.

[10] Gruber, M., Joseph, P., and Chong, T., "On the mechanisms of serrated airfoil trailing edge noise reduction," *17th AIAA/CEAS Aeroacoustics Conference (32nd AIAA Aeroacoustics Conference)*, , No. June, 2011, pp. 5–8. https://doi.org/10.2514/6.2011-2781, URL http://arc.aiaa.org/doi/10.2514/6.2011-2781.

[11] Arce León, C., Ragni, D., Pröbsting, S., Scarano, F., and Madsen, J., "Flow topology and acoustic emissions of trailing edge serrations at incidence," *Experiments in Fluids*, Vol. 57, No. 5, 2016. https://doi.org/10.1007/s00348-016-2181-1.

[12] Avallone, F., Pröbsting, S., and Ragni, D., "Three-dimensional flow field over a trailing-edge serration and implications on broadband noise," *Physics of Fluids*, Vol. 28, No. 11, 2016. https://doi.org/10.1063/1.4966633.

[13] Lima Pereira, L. T., Ragni, D., Avallone, F., and Scarano, F., "Aeroacoustics of sawtooth trailing-edge serrations under aerodynamic loading," *Journal of Sound and Vibration*, Vol. 537, No. April, 2022, p. 117202. https://doi.org/10.1016/j.jsv.2022.117202, URL https://doi.org/10.1016/j.jsv.2022.117202https://linkinghub.elsevier.com/retrieve/pii/S0022460X22003960.

[14] Chong, T. P., and Vathylakis, A., "On the aeroacoustic and flow structures developed on a flat plate with a serrated sawtooth trailing edge," *Journal of Sound and Vibration*, Vol. 354, 2015, pp. 65–90. https://doi.org/10.1016/j.jsv.2015.05.019, URL http://dx.doi.org/10.1016/j.jsv.2015.05.019.

[15] Jones, L. E., and Sandberg, R. D., "Acoustic and hydrodynamic analysis of the flow around an aerofoil with trailing-edge serrations," *Journal of Fluid Mechanics*, Vol. 706, 2012, pp. 295–322. https://doi.org/10.1017/jfm.2012.254.

[16] Taylor, G. I., "The Spectrum of Turbulence," *Proceedings of the Royal Society of London. Series A - Mathematical and Physical Sciences*, Vol. 164, No. 919, 1938, pp. 476–490. https://doi.org/10.1098/rspa.1938.0032, URL http://www.royalsocietypublishing.org/doi/10.1098/rspa.1938.0032.

[17] Ayton, L. J., Szoke, M., Paruchuri, C. C., Devenport, W. J., and Alexander, W. N., "Trailing-edge serrations: improving theoretical noise reduction models," *AIAA AVIATION 2021 FORUM*, American Institute of Aeronautics and Astronautics, Reston, Virginia, 2021. https://doi.org/10.2514/6.2021-2111, URL https://arc.aiaa.org/doi/10.2514/6.2021-2111.

[18] Sanjosé, M., Moreau, S., Lyu, B., and Ayton, L. J., "Analytical, numerical and experimental investigation of trailing-edge noise reduction on a Controlled Diffusion airfoil with serrations," *25th AIAA/CEAS Aeroacoustics Conference*, , No. May, 2019. https://doi.org/10.2514/6.2019-2450, URL https://arc.aiaa.org/doi/10.2514/6.2019-2450.

[19] Kholodov, P., and Moreau, S., "Optimization of trailing-edge serrations with and without slits for broadband noise reduction," *Journal of Sound and Vibration*, Vol. 490, 2020, p. 115736. https://doi.org/10.1016/j.jsv.2020.115736, URL https://doi.org/10.1016/j.jsv.2020.115736.

[20] van der Velden, W. C., Casalino, D., and Romani, G., "Full-Scale Serrated Wind Turbine Trailing Edge Noise Certification Analysis Based on the Lattice-Boltzmann Method," , No. January, 2023. https://doi.org/10.2514/6.2023-0970.

[21] Casalino, D., van der Velden, W., and Romani, G., "A Framework for Multi-Fidelity Wind-Turbine Aeroacoustic Simulations," *28th AIAA/CEAS Aeroacoustics Conference, 2022*, 2022. https://doi.org/10.2514/6.2022-2892.

[22] Luesutthiviboon, S., Ragni, D., Avallone, F., and Snellen, M., "An alternative permeable topology design space for trailing-edge noise attenuation," *International Journal of Aeroacoustics*, Vol. 20, No. 3-4, 2021, pp. 221–253. https://doi.org/10.1177/1475472X211003295.

[23] Christophe, J., Buckingham, S., Schram, C., and Oerlemans, S., "zEPHYR - Large On Shore Wind Turbine Benchmark," , 2022. https://doi.org/10.5281/zenodo.6380878, URL https://zenodo.org/record/6380879{#}.Y1ejH2dByUk.

[24] Roger, M., and Moreau, S., "Back-scattering correction and further extensions of Amiet's trailing-edge noise model. Part 1: Theory," *Journal of Sound and Vibration*, Vol. 286, No. 3, 2005, pp. 477–506. https://doi.org/10.1016/j.jsv.2004.10.054.

[25] Goody, M., "Empirical Spectral Model of Surface Pressure Fluctuations," *AIAA Journal*, Vol. 42, No. 9, 2008, pp. 1788–1794. https://doi.org/10.2514/1.9433.

[26] Kamruzzaman, M., Bekiropoulos, D., Lutz, T., Würz, W., and Krämer, E., "A Semi-Empirical Surface Pressure Spectrum Model for Airfoil Trailing-Edge Noise Prediction," *International Journal of Aeroacoustics*, Vol. 14, No. 5-6, 2015, pp. 833–882. https://doi.org/10.1260/1475-472x.14.5-6.833.

[27] Lee, S., and Villaescusa, A., "Comparison and assessment of recent empirical models for turbulent boundary layer wall pressure spectrum," *23rd AIAA/CEAS Aeroacoustics Conference, 2017*, , No. June, 2017, pp. 1–23. https://doi.org/10.2514/6.2017-3688.

[28] Rozenberg, Y., Robert, G., and Moreau, S., "Wall-pressure spectral model including the adverse pressure gradient effects," *AIAA Journal*, Vol. 50, No. 10, 2012, pp. 2168–2179. https://doi.org/10.2514/1.J051500.

[29] Corcos, G. M., "Resolution of Pressure in Turbulence," *The Journal of the Acoustical Society of America*, Vol. 35, No. 2, 1963, pp. 192–199. https://doi.org/10.1121/1.1918431.

[30] Hu, N., and Herr, M., "Characteristics of wall pressure fluctuations for a flat plate turbulent boundary layer with pressure gradients," *22nd AIAA/CEAS Aeroacoustics Conference, 2016*, 2016, pp. 1–18. https://doi.org/10.2514/6.2016-2749.

[31] Leloudas, G., "Optimization of Wind Turbines with respect to Noise," *Optimization*, , No. November, 2006.

[32] Chong, T. P., Joseph, P. F., and Davies, P. O., "Design and performance of an open jet wind tunnel for aero-acoustic measurement," *Applied Acoustics*, Vol. 70, No. 4, 2009, pp. 605–614. https://doi.org/10.1016/j.apacoust.2008.06.011, URL http://dx.doi.org/10.1016/j.apacoust.2008.06.011.

[33] Avallone, F., van der Velden, W. C., and Ragni, D., "Benefits of curved serrations on broadband trailing-edge noise reduction," *Journal of Sound and Vibration*, Vol. 400, No. April, 2017, pp. 167–177. https://doi.org/10.1016/j.jsv.2017.04.007, URL http://dx.doi.org/10.1016/j.jsv.2017.04.007.

[34] Avallone, F., van der Velden, W. C., Ragni, D., and Casalino, D., "Noise reduction mechanisms of sawtooth and combed-sawtooth trailing-edge serrations," *Journal of Fluid Mechanics*, Vol. 848, No. June, 2018, pp. 560–591. https://doi.org/10.1017/jfm.2018.377.

[35] Lima Pereira, L. T., Avallone, F., and Ragni, D., "Wall-pressure fluctuations over a serrated trailing edge at different angles of attack," *AIAA/CEAS Aeroacoustics Conference*, 2021, pp. 1–15. https://doi.org/10.2514/6.2021-2179.

[36] Lima Pereira, L. T., Avallone, F., Ragni, D., and Scarano, F., "A physics-based description and modelling of the wall-pressure fluctuations on a serrated trailing edge," *Journal of Fluid Mechanics*, Vol. 938, 2022, p. A28. https://doi.org/10.1017/jfm.2022.173, URL https://www.cambridge.org/core/product/identifier/S0022112022001732/type/journal{_}article.

[37] Buck, S., Oerlemans, S., and Palo, S., "Experimental characterization of turbulent inflow noise on a full-scale wind turbine," *Journal of Sound and Vibration*, Vol. 385, No. September 2016, 2016, pp. 219–238. https://doi.org/10.1016/j.jsv.2016.09.010, URL http://dx.doi.org/10.1016/j.jsv.2016.09.010.

[38] Churchfield, M. J., "A Method for Designing Generic Wind Turbine Models Representative of Real Turbines and Generic Siemens SWT-2.3-93 and Vestas V80 Specifications," 2012, pp. 1–28.

[39] "A parametric study of serration design for trailing–edge broadband noise reduction," *Work submitted to Applied Acoustics*, 2022. URL https://www.cambridge.org/core/product/identifier/S0022112022001732/type/journal{_}article.